SCIENTIFIC OASIS

Spectrum of Mechanical Engineering and Operational Research

Journal homepage: www.smeor-journal.org
eISSN: 3042-0288

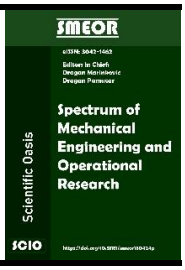

Numerical Study of Residual Stress Effects on Deformation and Fracture in Metal Matrix Composites

Ruslan Balokhonov[1,2 *], Aleksandr Zemlianov[1], Diana Gatiyatullina[1,2], Varvara Romanova[1,2]

[1] Institute of Strength Physics and Material Science, Russian Academy of Sciences, Tomsk, Russia
[2] Department of Solid Mechanics, Faculty of Physics and Engineering, National Research Tomsk State University, Tomsk, Russia

ARTICLE INFO

Article history:
Received 2 February 2025
Received in revised form 14 April 2025
Accepted 6 May 2025
Available online 15 May 2025

Keywords: Microstructure-based numerical simulation; Metal matrix composite materials; Residual stress; Fracture.

ABSTRACT

Composite materials used in various industries possess pronounced microstructural heterogeneity characterised by the difference in thermomechanical properties of the constituents and the presence of interfaces of different scales and geometries. In this study, the deformation and fracture of an aluminium alloy with a metal matrix composite coating under thermomechanical loading are numerically investigated at the micro-, meso- and macroscales. Complex microstructure of the composite material corresponding to the experimentally observed one is taken into account explicitly in the calculations. The constitutive equations for an isotropic elastic-plastic Al6061T6 matrix and elastic-brittle boron carbide particles are integrated into the ABAQUS/Explicit software package via user-defined subroutines. An energy-based fracture criterion formulated in terms of equivalent stresses is used to take into account the fracture of ceramic particles in local regions of tension or compression. The influence of residual stresses on the composite macroscopic strength, plastic strain localisation in the aluminum matrix and crack initiation and propagation in the particles is investigated under uniaxial tension or compression of the composite, with the volume fraction of particles in the coating being varied.

1. Introduction

Due to a unique combination of mechanical properties, such as high strength, hardness, wear and corrosion resistance, as well as low weight, composite materials and coatings are used in aerospace, energy, and automotive industries to produce critical parts [1-3]. Aluminum alloys are most often used as a matrix material for composites after steels [4]. Commercially pure aluminum has low yield and tensile strengths. To improve its performance, pure aluminum is alloyed by Cu, Mg, Mn, Si, Ni, Zn and other elements and thermally or mechanically treated [5]. Different ceramics are utilized for reinforcing metal-based composite coatings, with the most commonly used materials being boron carbides (B_4C), silicon carbides (SiC) and aluminum oxides (Al_2O_3) [6]. One of the key tasks is a proper selection of constituents [7]. Composites are produced by various

* *Corresponding author.*
E-mail address: rusy@ispms.ru

https://doi.org/10.31181/smeor21202537

methods: solid-state sintering [8], cold gas-dynamic spraying [9], stir casting [10, 11], squeeze casting [12], friction stir welding [13, 14], etc. Metal matrix composites and coatings manufactured by various methods possess a pronounced structural heterogeneity characterized by curvilinear interfaces between the coating layers, coating and substrate, metal matrix and reinforcing particles, as well as by the difference in the mechanical and thermal properties of the components (the elastic moduli, yield and ultimate tensile strengths, thermal expansion coefficients, etc.). In recent years, additive manufacturing of composites which can be treated as coating-by-coating product formation has been gaining popularity, primarily due to the growing industrial demand for complex-shaped products with a near-net shape structure and composition [15-18]. Review [17] presents the state-of-the-art of metal matrix composite additive manufacturing, including aluminum-based composites.

During manufacturing the composites and coatings accompanied by thermal cycling and high-temperature gradients, residual stresses may arise, which is considered as a negative factor, since the residual stresses can lead to rapid fracture of the product during loading, loss of geometric limits, significant deterioration of the performance and fatigue strength of the part [19].

In addition to experimental work related to the study of microstructure and mechanical properties of metal matrix composites and coatings, analytical [20] or numerical models [21, 22] are developed. Taking into account microstructural features in computational analysis of particulate-reinforced composites is important for an accurate prediction of the macroscopic response of the material under loading [23]. Extensive studies related to the evaluation of residual stresses and their influence on the mechanical behavior of composites are presented in the literature, for instance [22, 24]. The paper [22] presents several models for constructing the stress-strain curves of composites in the framework of a conventional mechanical strain gradient theory (CMSG), taking into account the residual stress and strain, grain refinement, «particle-matrix» interface debonding, brittle cracking of particles and viscous fracture of the metal matrix. Numerical and experimental investigations of residual stresses arising in sintered aluminum matrix gradient composites consisting of three layers with different volume fractions of particles were performed in [24]. Tensile or compressive residual stresses were found to arise in the AlSi12 matrix or Al_2O_3 and SiC particles.

Previously, disregarding residual stresses, we performed many-scale numerical and experimental studies of the deformation and fracture in an Al6061 alloy with an “aluminum matrix-carbide particles” coating [25] and in an additively manufactured Al-Si12 alloy treated as a hierarchical composite material [26]. Cooling induced residual stress effects on the deformation of an Al-Si12 alloy eutectics comprising a pure aluminum matrix with silicon particles were numerically investigated in [27]. This paper further extends the study [25] to address the influence of residual stresses on the deformation and fracture of an Al6061T6 substrate with a “Al6061T6 matrix - B_4C particles” composite coating across multiple spatial scales.

2. Thermomechanical Problem of Composite Deformation and Fracture

Figure 1a shows a SEM image of the cross-section of a coated material produced by laser cladding [28]. Metal matrix composite materials and coatings exhibit complex structure characterized by the interfaces of different scales and geometries influencing the composite deformation behavior. For accurate numerical predicting the composite response, two-phase model structures of the metal matrix coated material at different scales were created on the basis of the experimental image (Figure 1b-e).

At the macroscopic level of the aluminum substrate with composite coating, the characteristic scale is a few millimeters (Figure 1b), while the size of the coating material representative volume of a particulate-reinforced metal matrix composite at the meso-level is about hundreds of microns (Figure 1c). Previous studies have shown that at the mesoscale several particles undergo fracture simultaneously, and the strain localization in the aluminum matrix and fracture of ceramic particles develop in an interrelated manner [25]. At the micro-level of a single ceramic particle (Figure 1e) a hierarchy of fine structural heterogeneities could be singled out, which are oriented either along (region type A in Figure 1g) or perpendicular to the loading direction (region type B in Figure 1f), respectively. The characteristic size of an individual boron carbide particle is several tens of microns, while the size of A or B type interfacial asperities is on the order of a few microns.

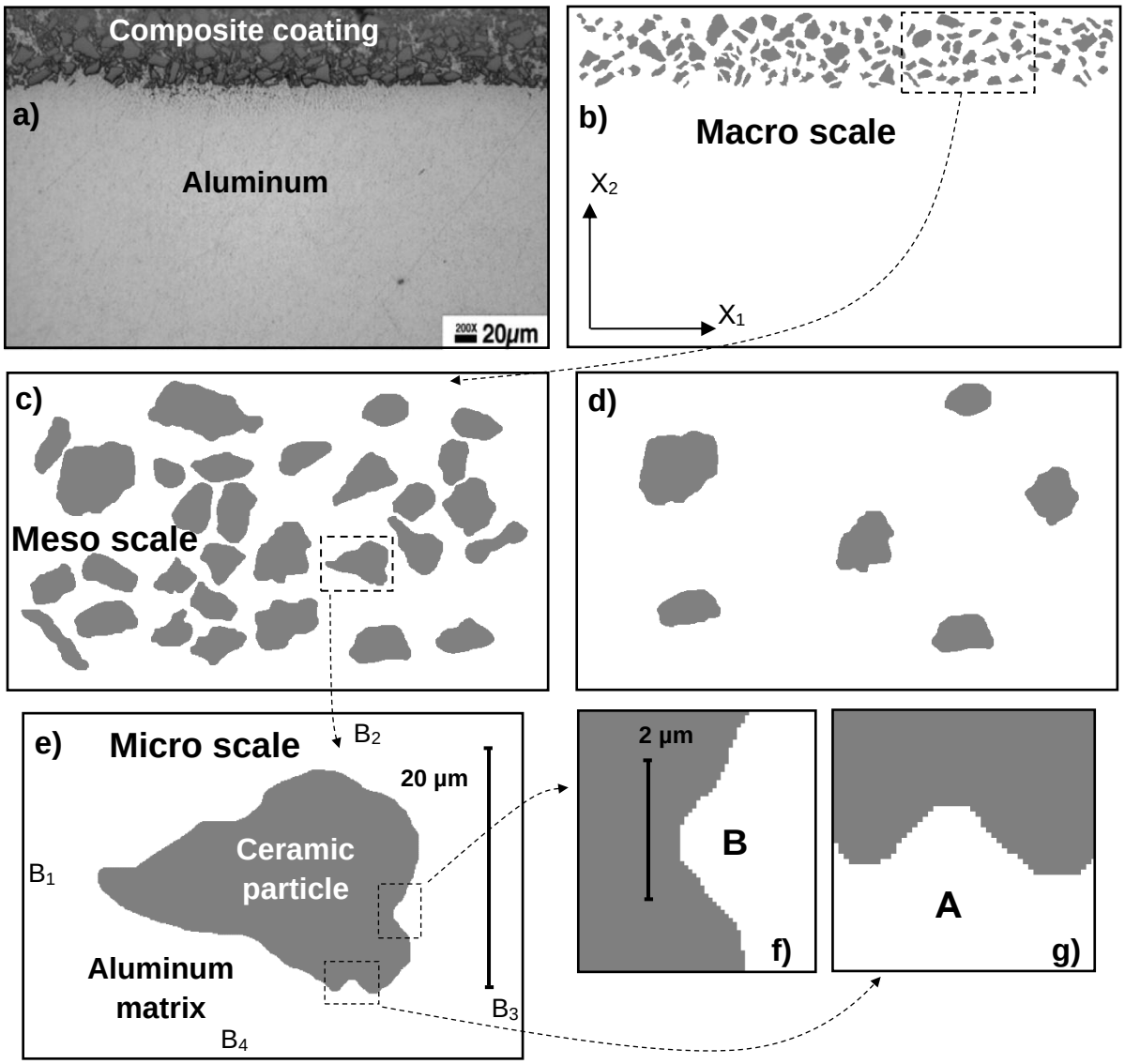

Fig. 1. Experimental image of the coated material (a) and model composites at different scales (b-g)

The general system of equations for continuum mechanics involving the laws of conservation of mass and momentum, as well as relations for the strain rates, is solved in a two-dimensional formulation using the finite element method. The Duhamel-Neumann relations were used to describe the thermoelastoplastic behavior of the composite:

$$\dot{\sigma}_{ij} = -\dot{P}\delta_{ij} + \dot{S}_{ij} = K(\dot{\varepsilon}_{kk} - 3\alpha\dot{T})\delta_{ij} + 2\mu(\dot{\varepsilon}_{ij} - \dot{\varepsilon}_{kk}\delta_{ij}/3 - \dot{\varepsilon}^{p}_{ij}) \quad (1)$$

where ε_{ij} and ε^{p}_{ij} are the total and plastic strain tensors, δ_{ij} is the Kronecker delta, K and μ are the bulk and shear elastic moduli, α is the thermal expansion coefficient, T is the temperature, the dot denotes the time derivatives.

Isotropic elastic-plastic and elastic-brittle models are used for the aluminium matrix and boron carbide particles, respectively. The plastic flow rule of aluminium is associated with the yield condition of Von Mises type including isotropic strain hardening function:

$$f_0\left(\varepsilon^{p}_{eq}\right) = \sigma_S - (\sigma_S - \sigma_0)\exp(-\varepsilon^{p}_{eq}/\varepsilon^{p}_{r}) \quad (2)$$

where σ_S and σ_0 are the ultimate and yield stress, ε^{p}_{r} is related to the strain hardening coefficient, and ε^{p}_{eq} are the accumulated equivalent plastic strain.

In order to model the particle cracking, an energy-based fracture criterion formulated in terms of the equivalent stress was chosen to take into account the type of local stress state in the material: bulk tension or compression.

$$\sigma_{eq} = \begin{cases} C_{ten}, & \text{if } \varepsilon_{kk} > 0 \\ C_{com}, & \text{if } \varepsilon_{kk} < 0 \end{cases} \quad (3)$$

where C_{ten} and C_{com} are the constants characterizing the ultimate tensile and compressive strengths of boron carbide, respectively. The thermomechanical properties of the aluminum matrix and boron carbide used in calculations are listed in Table 1.

Table 1
Thermomechanical properties of Al6061T6 and B_4C

Material	ρ, g/cm³	K, GPa	μ, GPa	σ_S, MPa	$\sigma_{0,2}$, MPa	ε_r^P, %	C_{ten}, MPa	C_{com}, GPa	α, 10^{-6} °C^{-1}
Al6061T6	2.7	66	26	332	234	9.5	-	-	22
B_4C	2.6	235	197	-	-	-	500	5	4.5

Dynamic boundary value problems for simulating the deformation of model structures at different scales are solved in a plane stress formulation by the finite element method. The constitutive equations (1)-(3) are integrated in ABAQUS/Explicit software package via user-defined subroutines.

For modeling the residual stress effects, the composite is initially cooled from the recrystallization temperature of aluminum to the room temperature, after which mechanical loading is applied. The same temperature throughout the computational domain decreases linearly. As a result of the cooling, residual stresses arise in the composite due to the difference in thermomechanical properties between the particle and matrix materials. During the cooling the boundaries B_1, B_2, B_3 and B_4 are free surfaces. Under uniaxial mechanical loading, the kinematic

boundary conditions are applied to B_1 and B_3 boundaries, while B_2 and B_4 boundaries are free of forces. To study the effect of the volume fraction of boron carbide on the cracking of the composite, an additional structure obtained from that shown in Figure 1c by sequentially removing several particles was created (Figure 1d). The volume fractions for the original structure shown in Figure 1c and the additional structure are 27% and 8%, respectively.

3. Numerical Simulation Results

3.1 Role of Matrix-Particle Interfacial Curvature at the Microscale

Let us consider the influence of cooling-induced residual stresses and type of loading on the crack propagation in composites. The numerical simulations were performed to solve four types of problems on loading the aluminum microvolume containing a single particle shown in Figure 1e:

1) compression from the initial undeformed state (Compression, C),
2) cooling followed by compression (Cooling followed by Compression, CC),
3) tension from the initial undeformed state (Tension, T),
4) cooling followed by tension (Cooling followed by Tension, TC).

Figure 2 shows the results of numerical simulations of crack initiation and propagation in the boron carbide particle under mechanical or thermomechanical loading of the composite. Presented are the pressure patterns, where the gray and red colors correspond to the maximum positive and negative pressure values, respectively. Corresponding stress-strain curves are demonstrated in Figure 3a. Here and further on in the graphs the stress $\langle\sigma\rangle$ was calculated as the equivalent stress averaged over the computational domain, while the strain ε corresponds to the relative elongation of the structure in the loading direction X_1. For the sake of comparing the mechanical and thermomechanical loadings, the stress-strain curves for the cases C and T start from the strain $\varepsilon = -0.7$ which is the average contraction of the composite after cooling.

At the microscale, the curvilinear interface between the B_4C particle and the aluminum matrix plays a decisive role in the crack initiation and propagation in the particle. Local regions of volumetric tensile stresses arise near the interfacial asperities oriented either along (type B regions under compression, Figure 2a) or perpendicular to the loading direction (type A regions under tension, Figure 2g). As the load increases, cracks nucleate in these regions and propagate parallel (Figure 2b) or perpendicular to the compression or tension direction (Figure 2h). The tensile stress concentration in the A type regions under tension is several times higher than that in the B-type regions under compression. As a result, the tensile strength of boron carbide $C_{ten} = 500\,\mathrm{MPa}$ is reached faster in T or TC than in C or CC cases, and the macroscopic strength of the microvolume both in terms of the stress and strain is higher under compression than under tension.

Let us compare the calculation results for C and CC loading types. In the C case the matrix is subjected to compressive stresses, whereas in the CC case at the beginning of compression after the cooling the matrix is almost completely under tension (compare Figures 2 a, d). Under further loading the stress state is gradually modified by decreasing the tensile stresses and increasing the compressive stresses in the matrix (Figure 2e, f). Crack initiation in the particle occurs earlier in the CC case than in the C case due to the additional contribution of compressive stresses arising during the composite cooling to the overall stress state in the composite. At the same time, the crack propagates slower for CC than for C loading type (cf. Figure 2a, b and d, e). At higher composite strain values in both loading cases a second crack nucleates at the opposite side of the particle and propagates towards the first crack (Figure 2c, f). The average stress level in the CC case is higher than in the C case during the whole compression except for the strain range from $\varepsilon = -0.8\%$ to

$\varepsilon = -1\%$ (dotted circle in Figure 3a). This is due to the earlier crack initiation under thermomechanical loading, as well as to the composite stress state modification slowing down the stress growth.

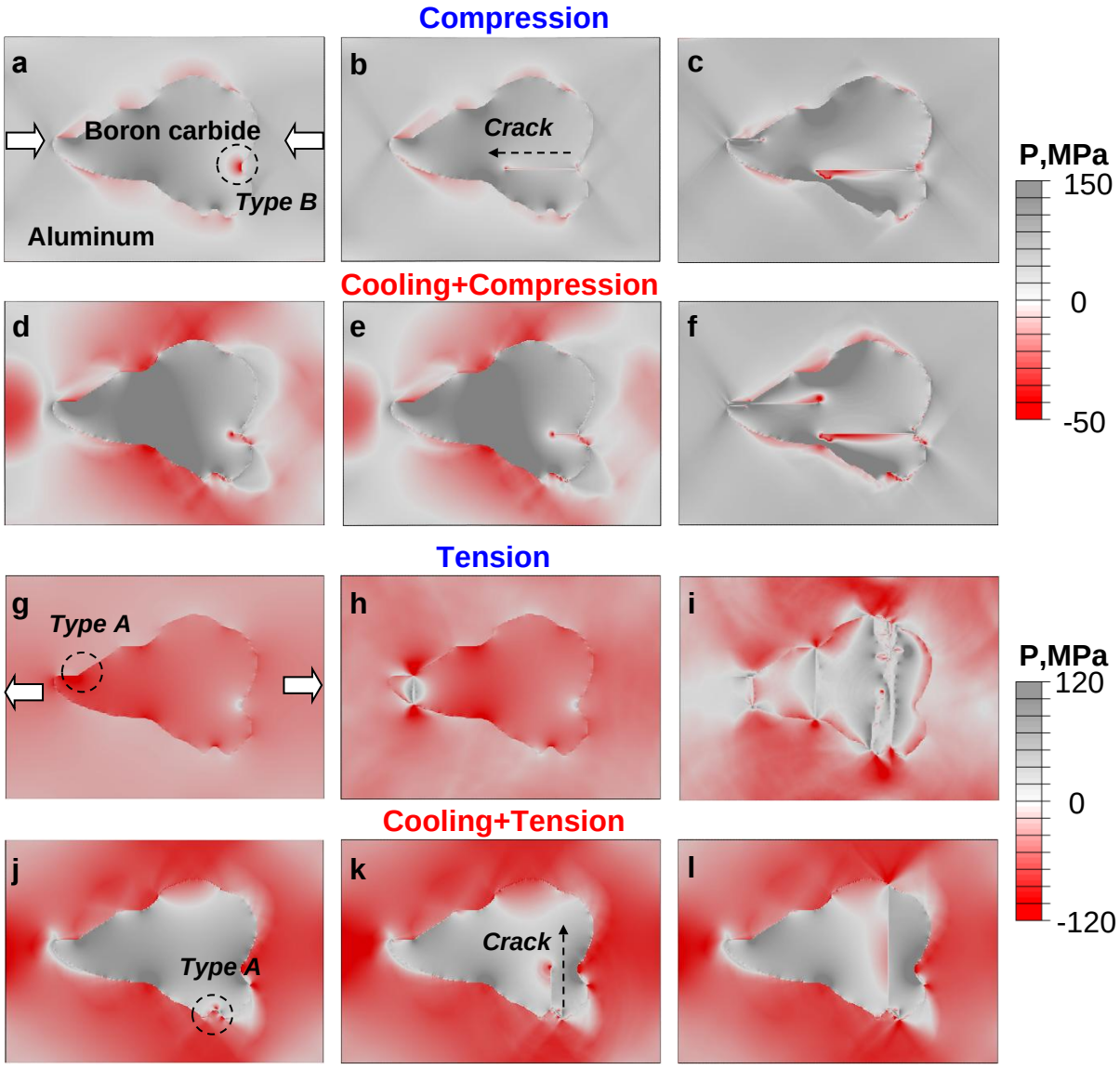

Fig. 2. Pressure distribution for the states **a-l** shown in Figure 3a

Let us study the deformation and fracture of the microvolume subjected to tension, at which cracks nucleate in the region of A-type asperities (Figure 2g, j). Similar to the compression (C- and CC- cases), fracture begins earlier in the TC case than for the T -type of loading (Figure 2 j). However, contrary to the compression cases, fracture in the T case nucleates near a different A-type asperity than in the TC case: first crack appears at the left side of the particle possessing needle-like shape, where high stress concentration is observed (Figure 2i). During further tension of the composite, several cracks form in the particle. The multiple cracking splits the particle into several fragments (Figure 2i), which causes a sharp stress drop in the stress-strain curve, significantly reducing the macroscopic strength of the composite (Figure 3a). It is interesting to note that in the TC case the crack initiation occurs in the boron carbide particle which is mostly volumetrically compressed: during the cooling the aluminum, whose thermal expansion coefficient

is higher than that of boron carbide, tends to compress the particle all-around (gray color in Figure 2 j). During further composite tension very local A-type tensile stress regions appear that initiates the tensile cracking in the compressed particle. Contrary to the T case crack propagation in the TC case does not cause a sharp stress drop in the stress-strain curve, because single crack propagates at lower velocity and the strain hardening of aluminum compensates the stress decreasing caused by fracture (Figure 3a).

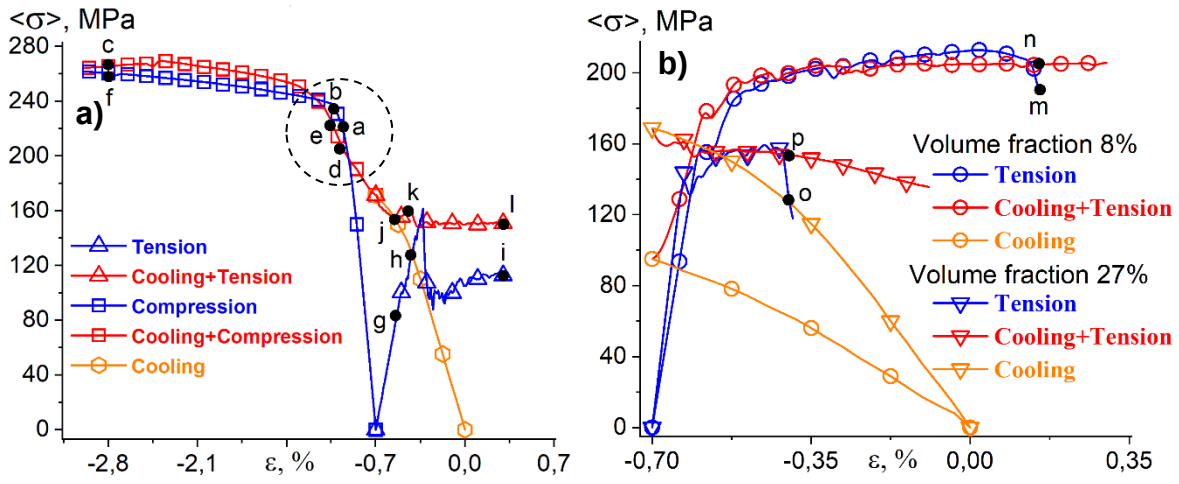

Fig. 3. Homogenized stress-strain curves of the composite with a single particle shown in Figure 1c (a) and with different particle volume fractions (8% and 27%) (b)

3.2 Effect of Particle Volume Fraction at the Mesoscale

At the mesoscale, in addition to the interface curvature, the volume fraction (VF) of boron carbide in the composite coating plays a significant role. Each particle contributes to the overall stress-strain state, and VF influences the deformation and fracture of a representative mesovolume of the composite coating. Figure 4 shows results of T and TC-type calculations for different VFs, and corresponding stress-strain curves for 8% and 27% VFs are presented in Figure 3b.

It was found that the macroscopic strength and relative elongation to fracture of the mesostructure are higher for 8% VF than for 27% VF (cf. the curves with triangles and circles in Figure 3b) that is true for both T and TC cases. The larger the VF, the higher the average stress level in the composite, the higher the stress concentration near the curvilinear interfaces, and that is why the earlier the particle fracture occurs. Moreover, the crack initiation and propagation occur more intensively for VF of 27%. Several particles located above each other relative to the direction of tension are fractured simultaneously, which results in a sharp stress drop in the stress-strain curve shown in Figure 3b, while several small stress drops are observed for VF of 8% due to the cracking of particles one by one (Figure 3b).

3.3 Effect of Coating-Substrate Interface at the Macroscale

Let us consider the thermomechanical behavior and fracture of Al6061T6 with composite metal matrix coating «Al6061T6-B_4C». In addition to the above mentioned effects of the interfacial curvature and volume fraction of particles, the interface between the composite coating and the aluminum substrate has a significant influence on the behavior of the coated material at the macroscopic scale. Figure 5 shows the stress-strain curves of the coated material for T (the blue curve with squares) and TC cases (the red curve with squares). After cooling, due to the difference in the thermal expansion coefficients of aluminum and boron carbide, plastic deformation is

localized near the curvilinear interfaces in the coating, with no plastic strains being observed in the aluminum substrate (Figure 5, state r). Due to the cooling induced plastic strain localization mainly around the boron-carbide particles, at the beginning of the coated material tension the average stress level is higher for TC than for T loading type. Under further loading, the stress-strain curves for TC and T cases intersect each other, and after that the current yield stress in the TC stress-strain curve becomes lower than the T stress due to the earlier fracture of the particles in the coated material subjected to tension after preliminary cooling (Figure 5, state r).

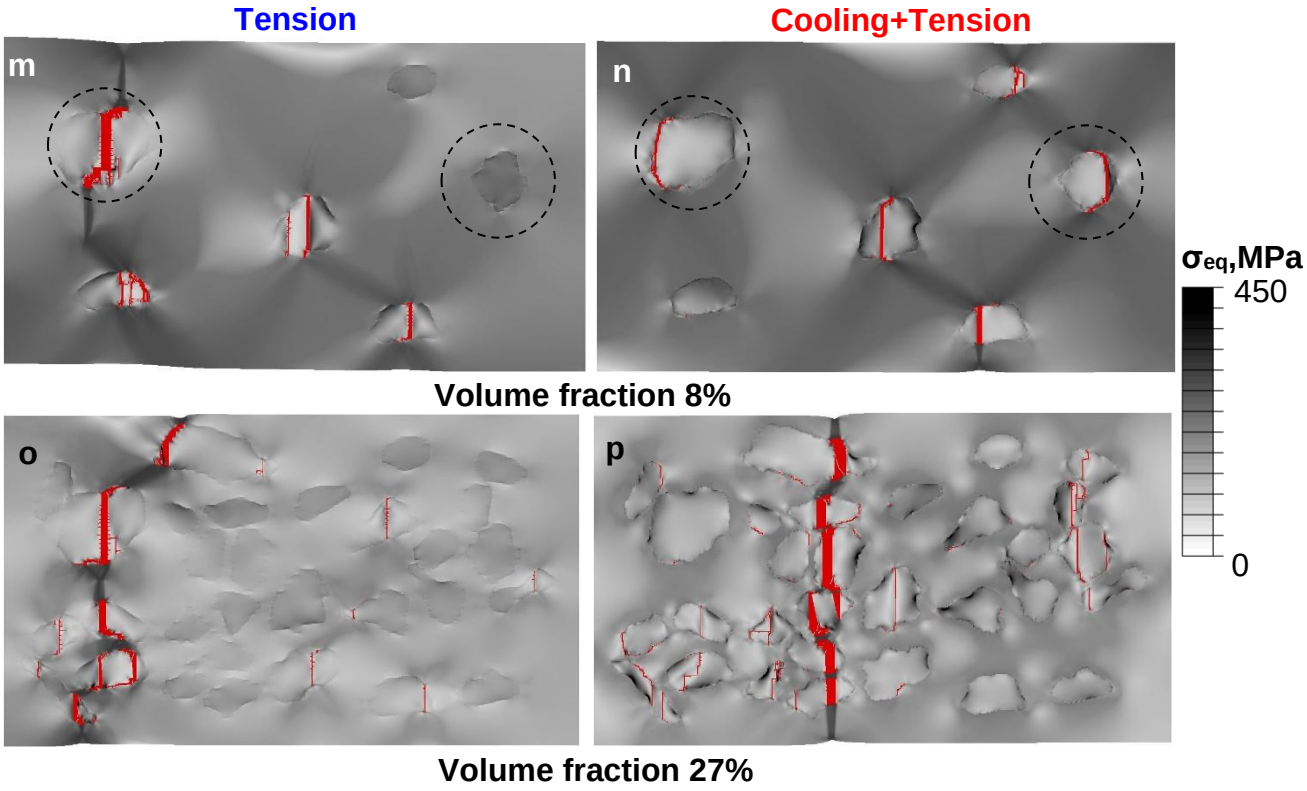

Fig. 4. Fracture patterns of the composites with particle volume fractions of 8% and 27%. **m-p** states are shown in Figure 3b. Red color indicates the fractured regions

Analysis of the fracture patterns (cf. states t and s in Figure 5) suggests the following conclusions. Firstly, several main cracks oriented perpendicular to the tensile direction is formed in the coating under both TC and T types of loading. The coating cracks with nearly regular intervals with the distance between the neighboring main cracks being greater for TC than for T case. Secondly, in T case the main cracks are of approximately the same thickness indicating that they form simultaneously, whereas in the TC case the cracks propagate consecutively during the coated material deformation. Finally, in TC case many secondary cracks in partially fractured particles located in between the primary main cracks are observed, whereas in the TC case there are much less particles completely fractured.

Cracks cause plastic strain localization in the aluminum substrate, with the main macroscopic shear bands being propagated at an angle of 60º to the loading axis from the primary crack tips formed at the coating-substrate interface (Figure 5, states t and s).

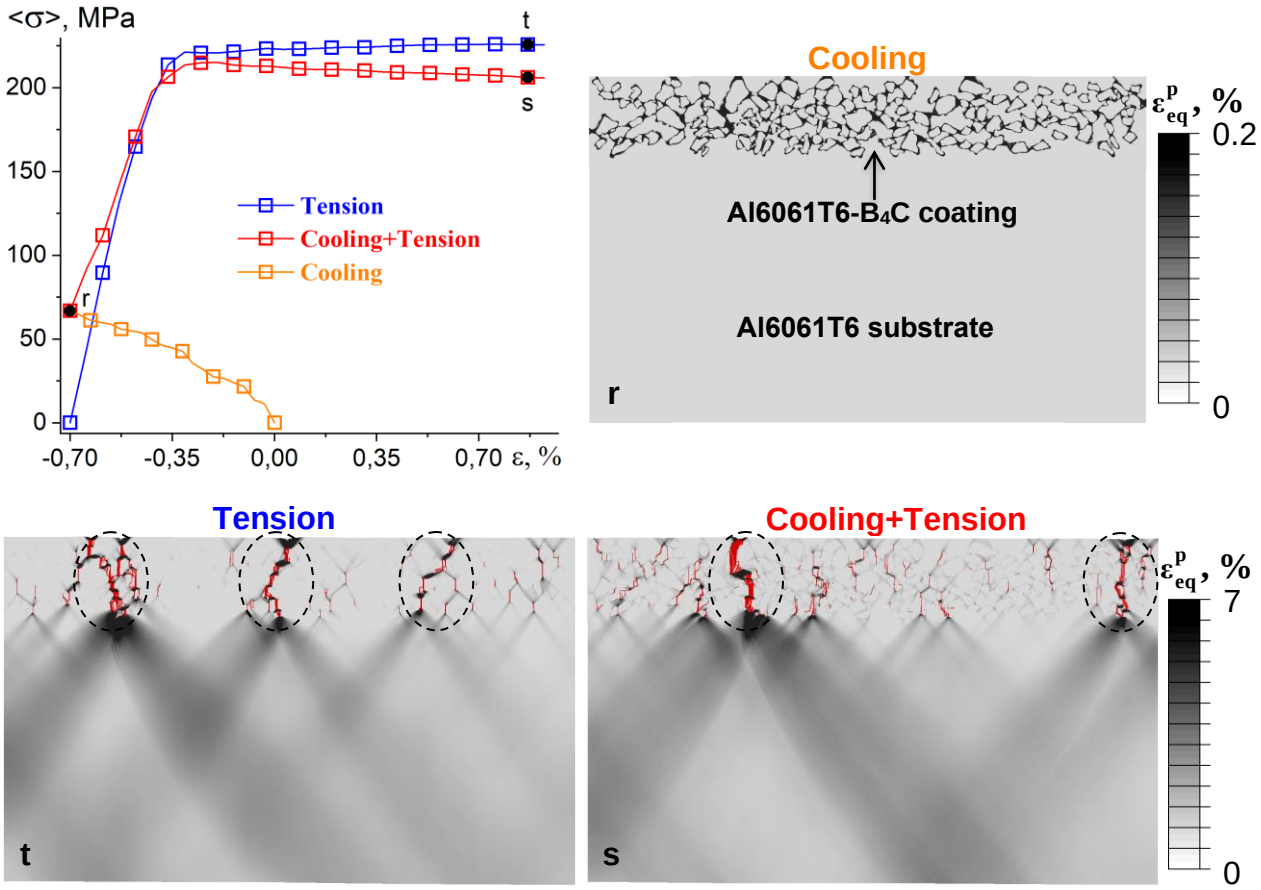

Fig. 5. Calculated stress-strain curves and plastic strain patterns of the material with a metal matrix composite coating shown in Figure 1b. Red color indicates fractured regions

4. Conclusions

Microstructure-based numerical simulation of deformation and fracture of an Al6061T6 substrate with a Al6061T6-B_4C metal-matrix composite coating has been performed at different spatial scales. An experimental image of the cross-section of the coated material manufactured by laser cladding method is used to take into account a complex microstructure of the composite material. Dynamic boundary-value problems for the composites are solved by the finite element method in ABAQUS/Explicit software package. The thermomechanical response of the composite, including isotropic elastic-plastic deformation of aluminum and elastic-brittle behavior of the boron carbide is modeled by the Duhamel-Neumann constitutive equation integrated into ABAQUS/Explicit via user subroutines. Residual stresses formed due to the difference in thermal expansion coefficients of aluminum and boron carbide are taken into consideration by preliminary cooling the composites from the recrystallization temperature of aluminum to the room temperature. Crack origination and growth in local regions of tensile stresses formed near the curvilinear matrix-particle interface during cooling with subsequent compression (CC) or tension (TC) of the aluminum microvolume containing a single boron carbide particle were studied. It was shown that crack initiation occurs near the interfacial asperities oriented perpendicular to the tension direction or along the compression direction. The crack initiation in the particle was shown to occur earlier under CC loading type than under compression of the uncooled composite (C) and, conversely, later in TC case than in T case which is the composite tension from the initial undeformed state. Cracks propagate slowly in CC or TC cases than in C or T cases, which is associated with the modification of the stress-strain state from volumetric during cooling to uniaxial

during subsequent mechanical loading. The combined effect of cooling-induced residual stresses and volume fraction of particles (VF) on the fracture and macroscopic strength of the composite was investigated at the mesoscale. The macroscopic strength and relative elongation to fracture of the mesovolume with 8% VF are higher than those for 27% VF. High stress concentration at 27% VF causes simultaneous fracture of several particles, whereas at VF of 27% the particles are fractured one by one in a successive manner. It was shown at the macroscale that the plastic strain localization and cooling-induced residual stresses arising in the composite coating substantially reduce the macroscopic strength of the coated material and cause formation of a few primary cracks and multiple secondary cracking in the coating.

Author Contributions

Conceptualization, R.B. and V.R.; methodology, R.B.; software, A.Z.; validation, D.G.; formal analysis, V.R.; investigation, R.B.; writing—original draft preparation, R.B. and A.Z.; writing—review and editing, R.B. and A.Z.; visualization, D.G. All authors have read and agreed to the published version of the manuscript.

Funding

The work was performed according to the Government research assignment for ISPMS SB RAS, project FWRW-2021-0002.

Data Availability Statement

All data generated or analyzed during this study are included in this published article. However, the reader may contact the corresponding author for more details on the data.

Acknowledgement

The work was performed according to the Government research assignment for ISPMS SB RAS, project FWRW-2021-0002.

Conflicts of Interest

The authors declare no conflicts of interest.

References

[1] Wu, X., & Zhang, W. (2024). A review on aluminum matrix composites' characteristics and applications for automotive sector. Heliyon, 10(1), Article e38576. https://doi.org/10.1016/j.heliyon.2024.e38576

[2] Nie, Z., Lu, H., Yang, F., & Xu, G. (2025). Preparation and property enhancement of SiC particle-reinforced aluminum matrix composites based on micro-arc oxidation. Journal of Alloys and Compounds, 1010, Article 177388. https://doi.org/10.1016/j.jallcom.2024.177388

[3] Singh, H., Brar, G. S., Kumar, H., & Aggarwal, V. (2021). A review on metal matrix composite for automobile applications. Materials Today: Proceedings, 43(1), 320–325. https://doi.org/10.1016/j.matpr.2020.11.670

[4] Ravi, L., Vanaraj, P. W., B. S, S., Perumal, S., Kumar, S., & Ravikirana. (2025). Enhancing mechanical and tribological properties of aluminum metal matrix composite reinforced with high entropy alloy using friction stir processing. Materials Chemistry and Physics, 338, Article 130614. https://doi.org/10.1016/j.matchemphys.2025.130614

[5] Garg, P., Jamwal, A., Kumar, D., Sadasivuni, K. K., Hussain, C. M., & Gupta, P. (2019). Advance research progresses in aluminium matrix composites: Manufacturing & applications. Journal of Materials Research and Technology, 8(5), 4924–4939. https://doi.org/10.1016/j.jmrt.2019.06.028

[6] Auradi, V., Rajesh, G. L., & Kori, S. A. (2014). Processing of B4C particulate reinforced 6061 aluminum matrix composites by melt stirring involving two-step addition. Procedia Materials Science, 6, 1068–1076. https://doi.org/10.1016/j.mspro.2014.07.177

[7] Fomin, V. M., Golyshev, A. A., Kosarev, V. F., Malikov, A. G., Orishich, A. M., & Filippov, A. A. (2020). Deposition of cermet coatings on the basis of Ti, Ni, WC, and B4C by cold gas dynamic spraying with subsequent laser irradiation. Physical Mesomechanics, 23, 291–300. https://doi.org/10.1134/S1029959920040025
[8] Chintada, S., Dora, S. P., Kare, D., & Doddi, P. R. V. (2021). Developments in sintered aluminium-based composites. Metal Powder Report, 76(6), 32–39. http://doi.org/10.1016/S0026-0657(21)00301-5
[9] Wu, D., Zhang, J., Li, W., Xu, Y., Yang, X., & Su, Y. (2024). Morphology of ceramic regulates the deposition behavior and mechanical properties of cold spray additive manufactured Al2O3/2024 aluminum matrix composites. Materials Characterization, 215(7), Article 114197. https://doi.org/10.1016/j.matchar.2024.114197
[10] Kumar, S. D., Ravichandran, M., Jeevika, A., Stalin, B., Kailasanathan, C., & Karthick, A. (2021). Effect of ZrB2 on microstructural, mechanical and corrosion behaviour of aluminium (AA7178) alloy matrix composite prepared by the stir casting route. Ceramics International, 47(9), 12951–12962. https://doi.org/10.1016/j.ceramint.2021.01.158
[11] Ahmad, S., Tian, Y., Hashmi, A. W., Singh, R. K., Iqbal, F., Dangi, S., Alansari, A., Prakash, C., & Chan, C. K. (2024). Experimental studies on mechanical properties of Al-7075/TiO2 metal matrix composite and its tribological behaviour. Journal of Materials Research and Technology, 30(1), 8539–8552. https://doi.org/10.1016/j.jmrt.2024.05.227
[12] Zhu, J., Jiang, W., Li, G., Guan, F., Yu, Y., & Fan, Z. (2020). Microstructure and mechanical properties of SiCnp/Al6082 aluminum matrix composites prepared by squeeze casting combined with stir casting. Journal of Materials Processing Technology, 283, Article 116699. http://doi.org/10.1016/j.jmatprotec.2020.116699
[13] Adetunla, A., Akinlabi, E., & Jen, T.-C. (2024). In-depth characterization of FSP-enhanced aluminum metal matrix: A study in materials modeling and computational techniques. Journal of Materials Research and Technology, 29, 5721–5730. https://doi.org/10.1016/j.jmrt.2024.02.229
[14] Liu, F. C., Feng, A. H., Pei, X., Hovanski, Y., Mishra, R. S., & Ma, Z. Y. (2024). Friction stir based welding, processing, extrusion and additive manufacturing. Progress in Materials Science, 146(1980–2015), Article 101330. https://doi.org/10.1016/j.pmatsci.2024.101330
[15] Lehner, P., Blinn, B., Zhu, T., Al-Zuhairi, A., Smaga, M., Teutsch, R., Beck, T. (2024). Influence of the as-built surface and a T6 heat treatment on the fatigue behavior of additively manufactured AlSi10Mg. International Journal of Fatigue, 187, Article 108479. https://doi.org/10.1016/j.ijfatigue.2024.108479
[16] Tang, S., Ummethala, R., Suryanarayana, C., Eckert, J., Prashanth, K. G., & Wang, Z. (2021). Additive manufacturing of aluminum-based metal matrix composites—A review. Advanced Engineering Materials, 23(7), Article 2100053. https://doi.org/10.1002/adem.202100053
[17] Nartu, M. S. K. K. Y., & Agrawal, P. (2025). Additive manufacturing of metal matrix composites. Materials & Design, Article 113609. https://doi.org/10.1016/j.matdes.2025.113609
[18] Zhu, Z., Hu, Z., Seet, H. L., Liu, T., Liao, W., Ramamurty, U., & Ling Nai, S. M. (2023). Recent progress on the additive manufacturing of aluminum alloys and aluminum matrix composites: Microstructure, properties, and applications. International Journal of Machine Tools and Manufacture, 190(5), Article 104047. https://doi.org/10.1016/j.ijmachtools.2023.104047
[19] Rashid, A., & Gopaluni, A. (2023). A review of residual stress and deformation modeling for metal additive manufacturing processes. Chinese Journal of Mechanical Engineering: Additive Manufacturing Frontiers, 2(4), Article 100102. https://doi.org/10.1016/j.cjmeam.2023.100102
[20] Yan, A., Zhang, H., Deng, B., Peng, F., Yan, R., & Cui, F. (2024). Analytical modeling of subsurface damage in laser-assisted machining of metal matrix composites based on the reinforcement fracture probability. *Journal of Manufacturing Processes, 109,* 300-312. https://doi.org/10.1016/j.jmapro.2023.12.001.
[21] Ma, S., Zhang, X., Chen, T., & Wang, X. (2020). Microstructure-based numerical simulation of the mechanical properties and fracture of a Ti-Al3Ti core-shell structured particulate reinforced A356 composite. Materials & Design, 19, Article 108685. http://doi.org/10.1016/j.matdes.2020.108685
[22] Wu, H., Xu, W., Shan, D., Wang, X., Guo, B., & Jin, B. C. (2023). Micromechanical modeling of damage evolution and fracture behavior in particle-reinforced metal matrix composites based on the conventional theory of mechanism-based strain gradient plasticity. Journal of Materials Research and Technology, 22, 625–641. https://doi.org/10.1016/j.jmrt.2022.11.139
[23] Ye, C., Wang, K., Ouyang, Q., Li, Z., & Zhang, D. (2024). Deformation and fracture of SiCp/Al composites under complex loading conditions: A simulation study. Journal of Materials Research and Technology, 30, 8137–8151. https://doi.org/10.1016/j.jmrt.2024.05.179
[24] Węglewski, W., Sequeira, A. A., Bochenek, K., Rosc, J., Brunner, R., & Basista, M. (2024). Finite element modeling of thermal residual stresses in functionally graded aluminum-matrix composites using X-ray micro-computed

tomography. Finite Elements in Analysis and Design, 241(4), Article 104239. https://doi.org/10.1016/j.finel.2024.104239

[25] Balokhonov, R. R., Romanova, V. A., & Schmauder, S. (2019). A numerical study of plastic strain localization and fracture across multiple spatial scales in materials with metal-matrix composite coatings. Theoretical and Applied Fracture Mechanics, 101, 342–355. https://doi.org/10.1016/j.tafmec.2019.03.013

[26] Balokhonov, R., Utyaganova, V., Gatiyatullina, D., Zemlianov, A., & Romanova, V. (2024). Interlayer effect on deformation and fracture of dendritic structure formed during wire-feed electron-beam additive manufacturing of Al-Si alloy. Facta Universitatis, Series: Mechanical Engineering, 22(3), 515–527. https://doi.org/10.22190/FUME240104009B

[27] Zemlyanov, A. V., Gatiyatullina, D. D., Utyaganova, V. R., & others. (2023). A study of deformation and fracture of the eutectic in an additively manufactured Al-Si composite. Physical Mesomechanics, 26(6), 678–690. http://doi.org/10.1134/S1029959923060073

[28] Kadolkar, P. B., Watkins, T. R., De Hosson, J. Th. M., Kooi, B. J., & Dahotre, N. B. (2007). State of residual stress in laser-deposited ceramic composite coatings on aluminum alloys. Acta Materialia, 55(4), 1203–1214. https://doi.org/10.1016/j.actamat.2006.07.049